Optimization of the Energy Input and Output Parameters for Pyroshock Testing

Alessandro Paolo Daga, Luca Viale, Alessandro Fasana

Optimization of the Energy Input and Output Parameters for Pyroshock Testing

Alessandro Paolo DAGA[1], Luca VIALE[1], Alessandro FASANA[1]

[1]Department of Mechanical and Aerospace Engineering, Politecnico di Torino,
Corso Duca degli Abruzzi 24, 10129 Torino, Italy
alessandro.daga@polito.it

Abstract

During the different phases of a mission, spacecraft equipment is subject to high-frequency shocks, commonly known as pyroshock since they are caused by explosive materials. The requirements for space qualification are usually expressed in terms of Shock Response Spectrum (SRS) acceleration – indicating the damage that a shock could potentially cause to a structure – and depend on the characteristics of the launch vehicles. Therefore, to simulate real shock load conditions in a repeatable and safe manner, hammers, projectiles, or generic impacting objects are commonly launched against a fixture (such as an anvil, a Hopkinson bar, or a resonant plate) supporting the component under test. This work exploits a numerical model entirely developed in the frequency domain which has been built to optimize the energy input and output parameters of a test facility. The development of the proposed model in the frequency domain contributes to considerable advantages, such as the reduction of calculation times. Based on the SRS requirements, the mass and speed of the bullet, the impact location, and the position of the object under test (mounted over a triangular plate) are comprehensively investigated by the proposed algorithm. Given the notable influence of these parameters and the complexity of their interactions, the proposed analysis considerably simplifies the tuning process, reduces calibration time and, in general, avoids costly trial-and-error repetitions.

1 Introduction

During the different phases of a mission, spacecraft equipment is subject to high-frequency shocks, commonly known as pyroshock as they are caused by explosive release charges. The important impulsive nature of such pyroshocks produces transient structural responses whose intensity could easily damage the carried equipment in the vicinity of the energy release zone. The requirements for space qualification are usually expressed in terms of Shock Response Spectrum (SRS) acceleration – indicating the damage that a shock could potentially cause to a structure [1,2] – and depend on the characteristics of the launch vehicles. In order to simulate real shock loads in a repeatable and safe manner, hammers, projectiles, or generic impacting objects are commonly launched against a fixture (in most of cases a resonant plate [3,4]) supporting the component under test, so as to reach the required SRS (as prescribed by the standards [5–8]).

The effect of the main test parameters over the resulting SRS was experimentally explored over the years [9,10], and several models were proposed such as Finite Element models (FEM) based on NASTRAN and DYTRAN [11], Statistical Energy Analysis (SEA) models [12,13], Transient Statistical Energy Analysis (TSEA) models [14,15], also combinable in Virtual Mode Synthesis and Simulation (VMSS) [16] or with FEM [17,18].

Unfortunately, such advanced models are too complex and computationally expensive to be used to automate the test parameters selection. In this respect, papers [19–21] proposed a simpler way to numerically simulate the behavior of the plate exploiting a simplified m-dof model of the plate, with lumped masses and stiffnesses, and a Frequency Domain Convolutional scheme, allowing a quick and reliable tuning of all the main test bench variables.

This work follows the paper [21] where the m-dof simplified model was substituted by a more advanced FEM to finally solve, in a fully automated way, the shape and size design of the plate based on some test requirements.

In this paper the same model is used to study the effect of the energy input and output parameters of a test facility in terms impact location, anvil material, and the mounting position of the object under test. In fact, given the notable influence of these parameters and the complexity of their interactions, a full parameters exploration can strongly reduce test calibration times while providing remarkable economic advantages, avoiding costly trial-and-error repetitions.

The complete model description is given in Section 2. The optimization results are reported and discussed in Section 3, while final conclusions will be derived in Section 4.

2 Methodology

In order to propose a fast yet accurate model for simulating the resulting SRS generated by a shock due to the hit of a projectile on an anvil mounted on the base plate, the methodology reported in [19–21] based on the physical model depicted in Figure 1 was adopted. In particular, the model is divided into 3 sub-models:

1. A FEM model of a plate with an anvil and a test object mounted in some points of the surface, able to compute the inertance of a metal plate of any shape and material at point *j* caused by an input at point *k*;
2. A numerical model for the impact, defining the input pulse signal as a function of the contact materials and projectile momentum in terms of mass and speed;
3. A numerical model for computing the maximax SRS with a Q factor of 10.

These three models are then merged by a Frequency Domain Convolutional scheme so as to speed up the procedure. From a practical point of view, the Convolution Theorem of the Fourier Transform is exploited, so as to produce the final equation:

$$SRS(\Omega_c) = \max\left(\mathrm{abs}\left(IFFT\left[F_j(\omega)\cdot I_{jk}(\omega)\cdot T_{SRS}^{\Omega_c}(\omega)\right]\right)\right) \tag{1}$$

where $F_j(\omega)$ is the impact force$F_j(\omega)$, $I_{jk}(\omega)$ is the plate Inertance $I_{jk}(\omega)$and $T_{SRS}^{\Omega_c}(\omega)$ is the Transmissibility of a SRS single degree of freedom with natural frequency Ω_c , as described in [21] and in the Figure 1 reported below.

$T_{SRS}^{\Omega_c}(\omega)$

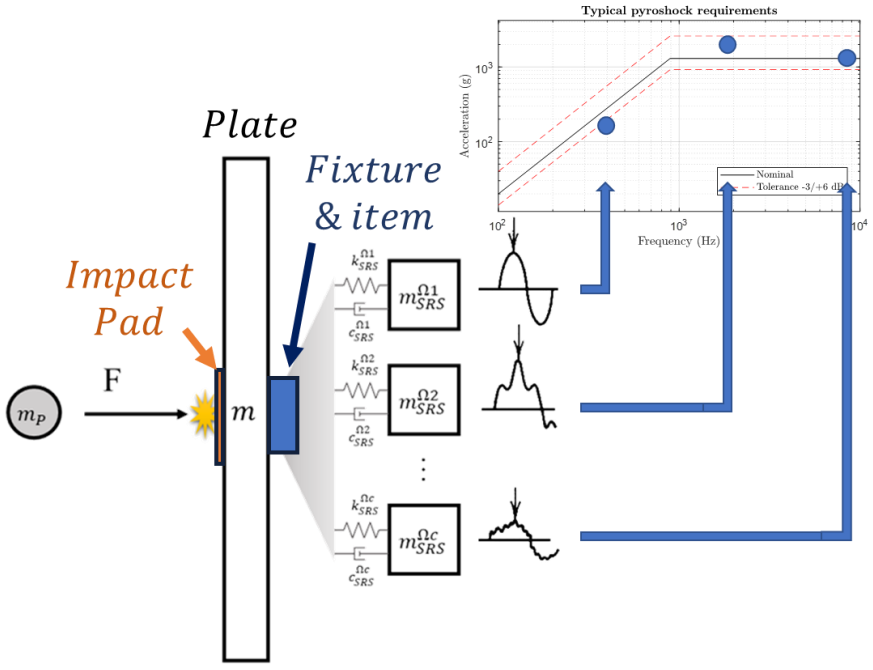

Figure 1: Physical model of a pyroshock test facility.

In this work, the plate shape and size are derived from [21], and the focus is on the possibility of obtaining a better match to the SRS requirement by varying the energy input and output parameters defined as the impact pad (or anvil) material, the impact location and the testing object mounting location (i.e., the acceleration measurement location) in the vicinity of their design values. The equilateral triangle plate of side dimension 1.04 m (i.e., inscribed in a circumference of 0.6 m) and thickness 0.04 m made of Aluminium was considered. Notice that this plate was automatically designed by the GA optimization algorithm in [21] without anvil nor testing object, whose influences were neglected, and considering an excitation and a measurement point coincident to the center of the plate. To simulate a real impulse, the impact force $f(t)$ is modelled by two half non-symmetrical windows (left and right) whose shape is defined as half a raised cosine (i.e., the von Hann window). The FE analysis for the bare triangular plate is reported in Figure 2.

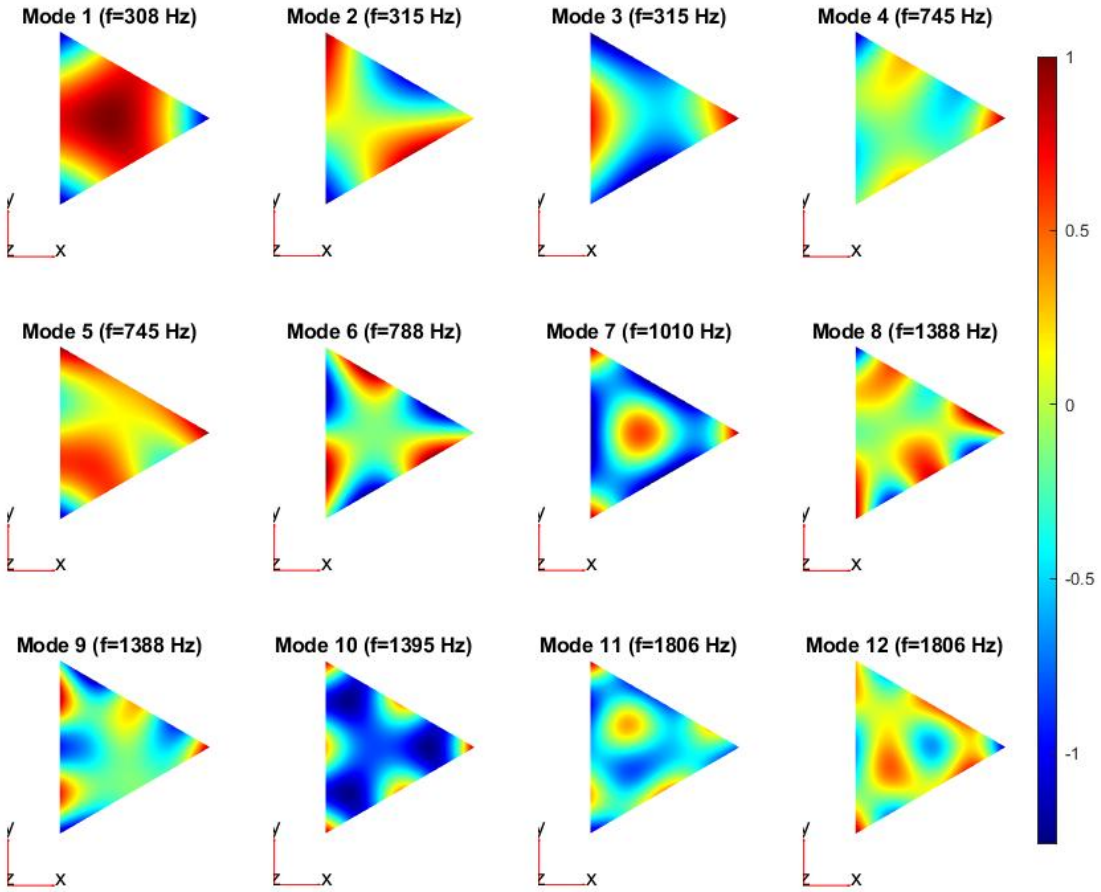

Figure 2: Modal analysis of the triangular plate.

Hence, in this work an anvil of fixed size 0.07x0.07x0.01 m^3 but variable material was defined. This clearly affects the Pulse Time computation as the anvil material can now be different from the plate material. At the same time, as a sample for the testing object, the NASA CubeSat 1U was selected, having an equivalent density of ρ_0 and a characteristic dimension (i.e., the side of the cube) of 0.1 m [22]. Finally, the input pulse location and the mounting location coordinates of the satellite were varied over a discrete range around the plate center (±0.1 m), as shown in Figure 3. Hence, a total of 162 combinations consisting of 9 input positions, 9 output positions, and 2 anvil plate materials are analyzed.

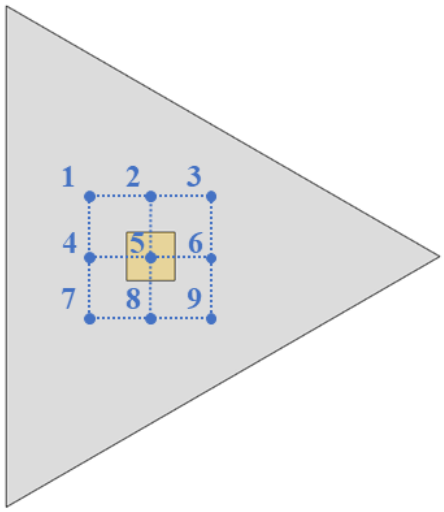

Figure 3: Scheme of the resonant plate (grey), specimen (yellow), and the 9 different position of input and output under analysis.

Parameter Name	Parameter Value / Range	Parameter Description
$\{u_i\}$	Points 1-9 (Figure 3)	Impact location coordinates
ρ_i	2700 or 7870 kg/m^3	Density of the anvil material
E_i	69 or 205 GPa	Young's modulus of the anvil material
ν_i	0.33 or 0.29	Poisson's ratio of the anvil material
σ_i	80 or 350 MPa	Yield stress of the anvil material
$\{u_0\}$	Points 1-9 (Figure 3)	Object location coordinates
ρ_0	2000 kg/m^3	Equivalent object density
l_0	0.1 m	Object characteristic dimension (side of the cube)
R	0.6 m	Radius of the circumscribed circle
n	3	Number of sides of the polygon
t	0.04 m	Thickness of the plate
$H_{min} - H_{max}$	0.0186 - 0.0373 m	Mesh size - range
ρ_p	2700 kg/m^3	Density of the plate material
E_p	69 GPa	Young's modulus of the plate material
ν_p	0.33	Poisson's ratio of the plate material
BC_s	Free	Type of Boundary conditions
$f_{min} - f_{max}$	100-10000 Hz	Range of frequency for the study
$\{w\}$	[0,0,1] (orthogonal)	Input Force intensity and direction
df	10 Hz	Frequency resolution for the Inertance
ζ_p	0.02	Modal damping factor of the plate
m_s	9 kg	Bullet mass
v_s	1 m/s	Bullet speed
R_s	0.2 m	Bullet contact radius
ρ_s	7870 kg/m^3	Density of the plate material
E_s	205 GPa	Young's modulus of the bullet
ν_s	0.29	Poisson's ratio of the bullet
sh	von Hann window	Window shape

Table 1: Whole model Parameters Description.

A list of the relevant parameters and their values is summarized in Figure 4 and Table 1. For further information refer to [21].

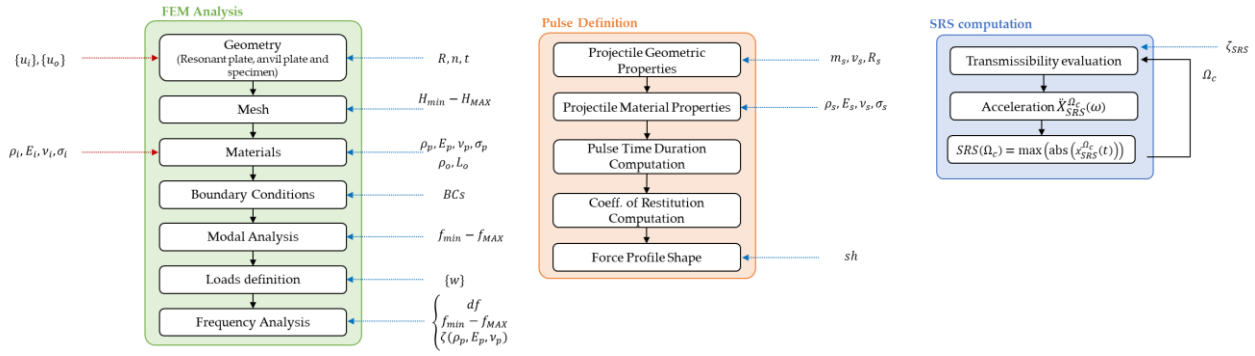

Figure 4: Whole model block scheme and parameters [21].

3 Results and Discussion

This analysis aims at investigating the possible optimization of the energy input and output parameters, given the geometry of the resonant plate. In fact, the plate adopted in this study has been optimized in terms of shape and size without considering the anvil plate and the object under test. Figure 5 shows the simulated SRS achievable considering only the resonant plate. It can be observed that the first peak coincides with the natural frequency of mode 1, while the second peak with mode 7. In fact, Figure 2 shows that modes 1 and 7 entail large displacements in the center of gravity (which coincides with the excitation and measurement points in this case).

By repeating the numerical simulation of the SRS per each of the 162 combinations under analysis, it is possible to observe how the energy input and output parameters influence the SRS with reference to the requirements and the related tolerances. A score function was defined as follows to evaluate how the configurations affect the goodness of the results:

$$score_{GA} = \begin{cases} log_{10}\left(\frac{\ddot{x}_{SRS}(\Omega_c)}{\ddot{x}_{req}(\Omega_c)}\right)^{log_{10}\left(\frac{\ddot{x}_{tol}^{+}(\Omega_c)}{\ddot{x}_{SRS}(\Omega_c)}\right)} & if\ \ddot{x}_{SRS}(\Omega_c) > \ddot{x}_{tol}^{+}(\Omega_c) \\ 0 & if\ \ddot{x}_{tol}^{-}(\Omega_c) < \ddot{x}_{SRS}(\Omega_c) < \ddot{x}_{tol}^{+}(\Omega_c) \\ log_{10}\left(\frac{\ddot{x}_{SRS}(\Omega_c)}{\ddot{x}_{req}(\Omega_c)}\right)^{log_{10}\left(\frac{\ddot{x}_{tol}^{-}(\Omega_c)}{\ddot{x}_{SRS}(\Omega_c)}\right)} & if\ \ddot{x}_{SRS}(\Omega_c) < \ddot{x}_{tol}^{-}(\Omega_c) \end{cases} \quad (2)$$

where $\ddot{x}_{SRS}(\Omega_c)$ is the calculated value of the acceleration synchronized to the resonant frequency Ω_c of the c-th s-dof system for the SRS calculation, $\ddot{x}_r(\Omega_c)$ is the test requirement (or the generic reference curve) in terms of SRS acceleration, $\ddot{x}_{tol}^{-}$ and $\ddot{x}_{tol}^{+}$ are respectively the values of the lower and upper tolerances. The proposed score function aims at evaluating the error only when the SRS falls outside the tolerances region, penalizing more undertesting conditions than overtesting. For the sake of clarity, Figure 6 shows the colormap representing the score applied to the SRS predictions, considering a standard requirement.

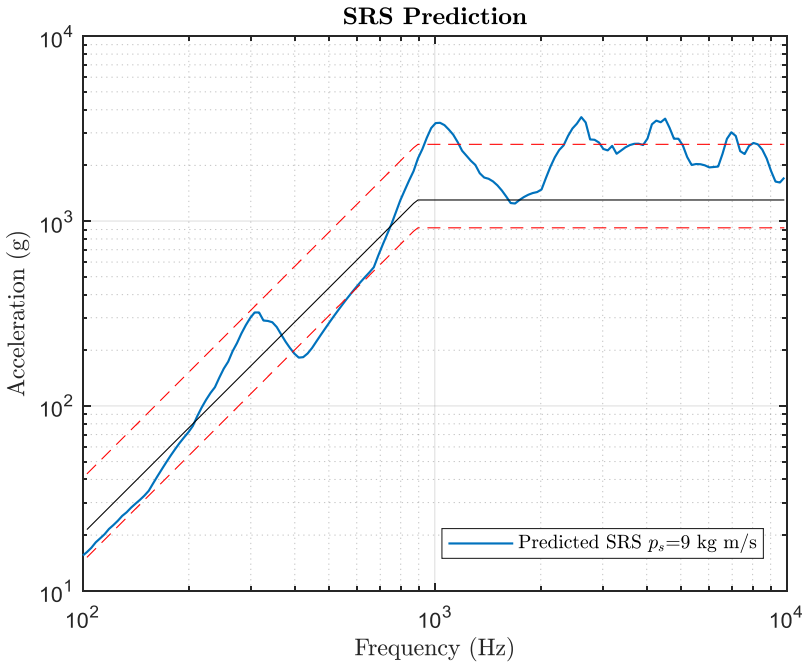

Figure 5. Simulated SRS inherent to the GA-optimized resonant plate.

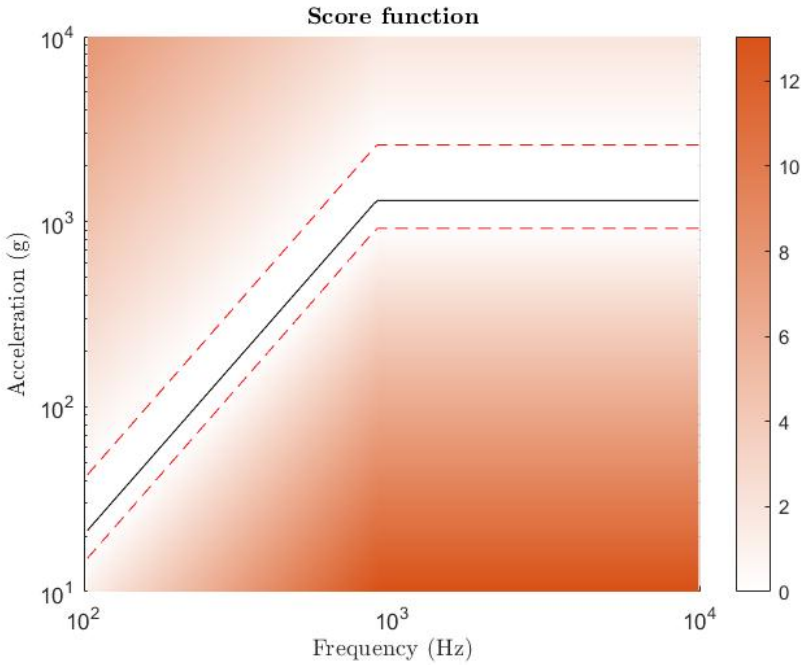

Figure 6: Colormap describing the adopted score function according to the specified requirements and the related tolerances.

The scores obtained with Eq. (2) referring to each of the 162 conditions are shown in Figure 7. It is worth noting that the steel anvil plate performs better than the aluminum one. This is probably due to the restitution coefficient e and the pulse duration τ, which depend on the mechanical properties of the impacting bodies. Furthermore, it can be observed that setting #41 (i.e., conditions used to optimize the plate design in [21]) remains the best one among the aluminum anvil plates. The equivalent condition with the steel anvil plate corresponds to setting #122, while the overall best case is #131. This was obtained by setting the input to coordinates (0 m; 0 m) and the specimen in point 6 (0.1 m; 0 m).

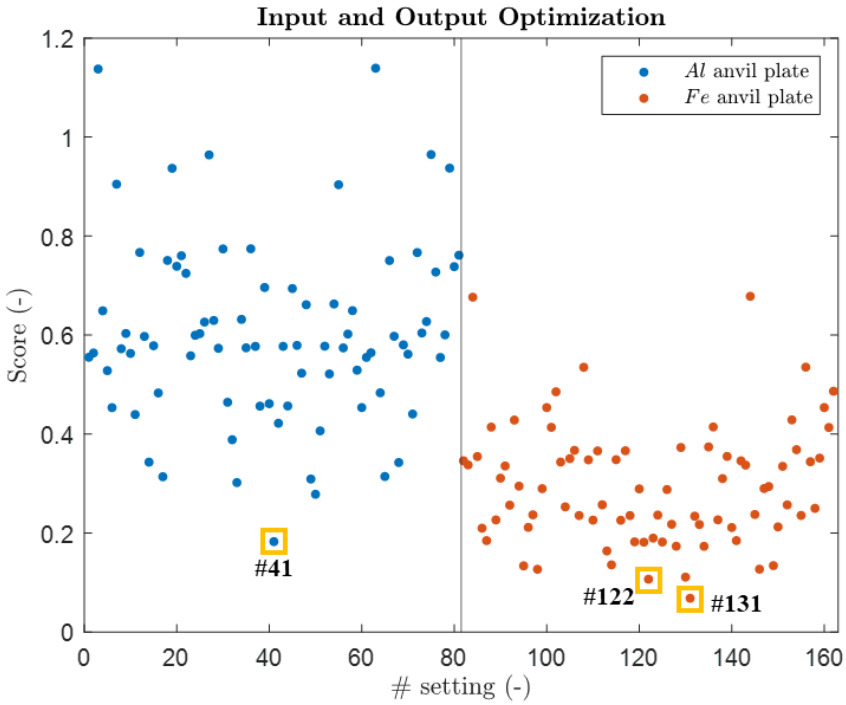

Figure 7: Score inherent to the 162 analysed setting conditions.

Finally, Figure 8 shows the predicted SRS in the three most interesting configurations: #41, #122, and #131. The best condition #131 leads to meeting the requirements very satisfactorily. Furthermore, comparing the three curves obtained with the bare plate SRS simulation in Figure 2, the peak at about 308 Hz is missing due to the introduction of the anvil plate and the specimen.

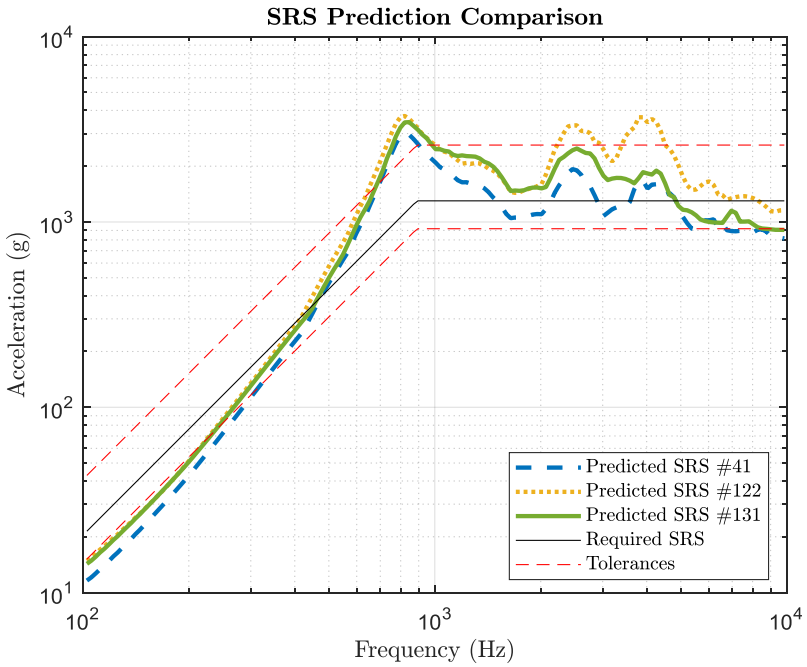

Figure 8: Comparison of the predicted SRS obtained with settings #41 (condition optimized in [21]), #122 (condition optimized in [21] with a steel anvil plate), and #131 (energy input and output optimized configuration).

4 Conclusions

The present work investigates the effect of the energy input and output parameters of a test facility in terms impact location, anvil material, and the mounting position of the object under test. A numerical model entirely developed in the frequency domain has been exploited to comprehensively examine all the possible configurations with a high degree of accuracy and reduced calculation times. The results showed that it is possible to obtain a configuration that better meets the requirements by optimizing the energy input and output parameters. Indeed, the SRS predicted in the optimized condition faithfully falls within the tolerance range. Given the notable influence of these parameters and the complexity of their interactions, the obtained results allow to considerably reduce calibration times during the tuning process and, in general, to avoid costly trial-and-error repetitions.

References

[1] C.M. Harris, A.G. Piersol, Harris' shock and vibration handbook, McGraw-Hill New York, 2002.

[2] A. Calvi, G. Aglietti, J. Albus, M. Bellini, D. Burtin, E. Cavro, J. Dupré, C. Fabriés, S. Fransen, D. Gangloff, A. Girard, N. Gualtieri, A. Itta, G. Kerschen, W. Konrad, R. Morisset, P. Nali, A. Newerla, G. Quagliotti, A. Rittweger, N. Roy, G. Sinnema, R. Ullio, J. Vergniaud, R. Veul, J. Wijker, ECSS-E-HB-32-26A Spacecraft Mechanical Loads Analysis Handbook, Undefined. (2013).

[3] J.-R. Lee, C.C. Chia, C.-W. Kong, Review of pyroshock wave measurement and simulation for space systems, Measurement. 45 (2012) 631–642. https://doi.org/10.1016/j.measurement.2011.12.011.

[4] Y. Yan, Q.M. Li, A pyroshock signal characterization method based on shock-waveform dictionary, Int. J. Mech. Sci. 249 (2023) 108251.

[5] H. Himelblau, Pyroshock Test Criteria, NASA-STD-7003A, 2011.

[6] MIL-STD-810F, Dep. Def. Test Method Stand. Environ. Eng. Consid. Lab. Tests Version F US Gov. Print. Off. (2000).

[7] A.P. One, Pyroshock Testing Techniques, (2009).

[8] E.S.A. ECSSSecretariat, R. ESTEC, ECSS-E-ST-10-03C, Space Eng.-Test. ESA Publ. Div. Noordwijk Neth. (2012).

[9] M. Jonsson, Development of a shock test facility for qualification of space equipment, Dep. Appl. Mech. Göteb. Swed. (2012).

[10] C. Sisemore, M.A. Spletzer, Design of a Resonant Plate Shock Fixture to Attenuate Excessive High-Frequency Energy Inputs., Sandia National Lab.(SNL-NM), Albuquerque, NM (United States), 2017.

[11] S. Kiryenko, G. Piret, J. Kasper, ESA/ESTEC shock bench presentation, in: Spacecr. Struct. Mater. Mech. Test. 2005, 2005.

[12] F.J. Fahy, Statistical energy analysis: a critical overview, Philos. Trans. R. Soc. Lond. Ser. Phys. Eng. Sci. 346 (1994) 431–447.

[13] C.B. Burroughs, R.W. Fischer, F.R. Kern, An introduction to statistical energy analysis, J. Acoust. Soc. Am. 101 (1997) 1779–1789.

[14] R.J. Pinnington, D. Lednik, Transient statistical energy analysis of an impulsively excited two oscillator system, J. Sound Vib. 189 (1996) 249–264.

[15] B.Y. Mao, S.L. Xie, M.L. Xu, X.N. Zhang, G.H. Zhang, Simulated and experimental studies on identification of impact load with the transient statistical energy analysis method, Mech. Syst. Signal Process. 46 (2014) 307–324.

[16] E. Dalton, B. Chambers, I.I. Chambers, Analysis and validation testing of impulsive load response in complex, multi-compartmented structures, in: 36th Struct. Struct. Dyn. Mater. Conf., 1995: p. 1243.

[17] R. Ullio, P.C. Marucchi-Chierro, A. Spazio, Utilization of prediction methods in the shock environment evaluation, in: Spacecr. Struct. Mater. Mech. Test., 2001: p. 239.

[18] X. Wang, W. Liu, J. Ding, Y. Sun, Y. Dang, Pyroshock Response Prediction of Spacecraft Structure in Wide Frequency Domain Based on Acceleration FRF, Aerospace. 9 (2022) 54.

[19] L. Viale, A.P. Daga, L. Garibaldi, A. Fasana, Numerical Modeling of a Pyroshock Test Plate for Qualification of Space Equipment, in: P. Rizzo, A. Milazzo (Eds.), Eur. Workshop Struct. Health

Monit., Springer International Publishing, Cham, 2023: pp. 990–999. https://doi.org/10.1007/978-3-031-07322-9_100.
[20] D. Alessandro Paolo, V. Luca, G. Luigi, F. Alessandro, M. Stefano, Frequency Domain Convolutional Model of a Pyroshock Plate for Qualification of Space Equipment, IC-MSQUARE-2022 AIP Conf. Proc. Vol. 2872. (2022).
[21] L. Viale, A.P. Daga, L. Garibaldi, Design of a Resonant Plate for Pyroshock Testing based on Shape and Size Heuristic Optimization, Survishno 2023 Conf. Proc. (2023).
[22] Stanford University and California Polytechnic Institute, CubeSat Design Specifications Document, Revision 14, (2020). https://static1.squarespace.com/static/5418c831e4b0fa4ecac1bacd/t/5f24997b6deea10cc52bb016/1596234122437/CDS+REV14+2020-07-31+DRAFT.pdf.